

Research Article

Isolation, Crystal Structure, and *In Silico* Aromatase Inhibition Activity of Ergosta-5, 22-dien-3 β -ol from the Fungus *Gyromitra esculenta*

Yerlan Melsuly Suleimen ^{1,2}, Ahmed M. Metwaly ³, Ahmad E. Mostafa ³,
Eslam B. Elkaeed ⁴, Hong-Wei Liu ⁵, Buddha Bahadur Basnet ⁶,
Raigul Nurbekkyzy Suleimen ⁷, Margarita Yulayevna Ishmuratova,⁸
Koblandy Muboryakovich Turdybekov ⁹ and Kristof Van Hecke ¹⁰

¹Sh. UalikhanovKokshetau University, Kokshetau, Kazakhstan

²Republican Collection of Microorganisms, Nur-Sultan, Kazakhstan

³Pharmacognosy and Medicinal Plants Department, Faculty of Pharmacy, Al-Azhar University, Cairo, Egypt

⁴Department of Pharmaceutical Sciences, College of Pharmacy, AlMaarefa University, Ad Diriyah, Riyadh 13713, Saudi Arabia

⁵State Key Laboratory of Mycology, Institute of Microbiology, Chinese Academy of Sciences, Beijing 100101, China

⁶Faculty of Sciences, Nepal Academy of Science and Technology, Khumaltar, Lalitpur, Nepal

⁷L.N. Gumilyov Eurasian National University, Nur-Sultan, Kazakhstan

⁸E. A. Buketov Karagandy University, Karaganda, Kazakhstan

⁹Department of Physics of Academician E.A. Buketov Karaganda University, Karaganda 100028, Kazakhstan

¹⁰XStruct, Department of Chemistry, Ghent University, Ghent B-9000, Belgium

Correspondence should be addressed to Yerlan Melsuly Suleimen; syerlan75@yandex.kz and Ahmed M. Metwaly; ametwaly@azhar.edu.eg

Received 12 March 2021; Revised 7 July 2021; Accepted 10 July 2021; Published 16 August 2021

Academic Editor: Wagdy Eldehna

Copyright © 2021 Yerlan Melsuly Suleimen et al. This is an open access article distributed under the Creative Commons Attribution License, which permits unrestricted use, distribution, and reproduction in any medium, provided the original work is properly cited.

Ergosterol derivatives exhibited copious promising biological activities. The fungus *Gyromitra esculenta* is widely distributed in Europe and North America. In order to examine the chemical properties of *Gyromitra esculenta*, a phytochemical study has been preceded and resulted in the isolation of the steroid, ergosta-5, 22-dien-3 β -ol (brassicasterol), from its methanol extract. The complete identification and absolute configuration of the isolated compound have been established by X-ray structural analysis to be (22E, 24R)-24-methylcholesta-5, 22-dien-3 β -ol. The reported cytotoxicity and the great structural similarity of the isolated compound with the cocrystallized ligand of the aromatase enzyme inspired us to run molecular docking studies against that protein. Ergosta-5, 22-dien-3 β -ol occupied the target protein with a binding mode almost the same as the cocrystallized ligand and a binding affinity of -33.55 kcal/mol, which was better than that of the cocrystallized ligand (-22.61 kcal/mol). This promising result encouraged us to conduct *in silico* ADMET and toxicity studies of ergosta-5, 22-dien-3 β -ol against 6 models, and the results expected the likeness of the isolated compound to be a drug. In conclusion, ergosta-5, 22-dien-3 β -ol has been isolated from *Gyromitra esculenta*, identified by X-ray structural analysis, and exhibited promising *in silico* activities against aromatase enzyme.

1. Introduction

Natural products are the key source that humankind relied on to treat diseases and maintain good health [1, 2]. The effective secondary metabolites that are responsible for

natural products' activity could be derived from plants [3, 4] or marines [5, 6]. Furthermore, fungi represent an unlimited origin of bioactive metabolites [7–13]. The isolated bioactive metabolites could be classified regarding their chemical classes to be flavonoids [14–17], saponins

[18, 19], isoflavonoids [20], sesquiterpene lactones [21], diterpenes [22], pyrones [23], alkaloids [24, 25], and steroids [26].

Gyromitra esculenta is a fungus that belongs to the genus *Gyromitra* which is widely distributed across Europe and North America. It normally fruits in spring and early summer in sandy soils under the coniferous trees. The fruiting body (mushroom) is an irregular brain-shaped dark brown cap that can reach 10 cm in height and 15 cm in width, perched on a stout white stipe up to 6 cm in height [27, 28]. Despite the reported toxicity of *G. esculenta*, it is still consumed and used in some countries in North America and Europe due to its high nutritive value [29, 30].

Ergosterol and its derivatives were reported to have various cytotoxic effects. As an example, ergosterol could inhibit *in vitro* and *in vivo* cancer growth through upregulation of multiple tumor suppressors [31, 32]. Furthermore, ergosterol peroxide exerted promising antitumor activities in colorectal cancer [33] and several other tumor types [34]. Additionally, dehydroergosterol derivatives induced apoptosis in human malignant melanoma cells [35] and inhibited the growth of human breast adenocarcinoma MCF-7 cells [36]. Interestingly, a dehydroergosterol derivative isolated from *Ganoderma lucidum* inhibited the proliferation of human cervical carcinoma cells with an IC_{50} value of $8.58 \mu\text{M}$ through induction of apoptosis [37]. Some ergosterol derivatives displayed anticancer activities through the inhibition of aromatase protein [38, 39].

Compound **1** (brassicasterol) has been isolated before from several plant sources such as the steam distillate of rapeseed oil [40] and *Brassica juncea* seeds [41]. Moreover, it was found in algae [42] and marine organisms [43]. In addition to the anti-inflammatory effect [44], brassicasterol could inhibit bladder carcinogenesis in an *in vivo* study [45].

X-ray crystallography is the technique that uses the ability of X-rays to be diffracted by a crystalline structure into different specific directions. The angles and intensities of the diffracted X-ray beams could be used to determine the three-dimensional picture of the electron density of the diffracting crystal. Consequently, the atoms' positions, chemical bonds, absolute configuration, and several other information can be determined [46].

Herein, we discuss the isolation, crystal structure, and molecular docking of ergosta-5, 22-dien-3 β -ol against the aromatase enzyme.

2. Results and Discussion

2.1. Isolation and Identification of Brassicasterol (Compound 1). Brassicasterol (Figure 1 and Table 1) was isolated from *G. esculenta* using different chromatographic techniques and identified as (22E, 24R)-24-methylcholesta-5, 22-dien-3 β -ol (ergosta-5, 22-dien-3 β -ol) or brassicasterol. The compound was identified by comparing its 1D and 2D NMR spectroscopic spectra with the published data (supplementary materials, Figures S1–S5) [44, 47].

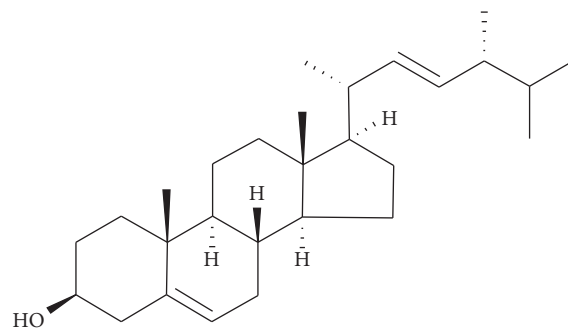


FIGURE 1: Chemical structure of compound **1**.

TABLE 1: C NMR data of brassicasterol in CDCl_3 compared with the reported literature [13].

C	δ C of 1	Reported δ C [47]	C	δ C of 1	Reported δ C [47]
1	37.4	37.4	15	24.4	24.4
2	30.1	29.9	16	28.7	28.7
3	72.0	72.0	17	56.2	56.2
4	42.4	42.4	18	12.2	12.2
5	140.9	140.9	19	19.5	19.6
6	121.9	121.9	20	40.3	40.3
7	32.0	31.8	21	21.1	21.1
8	32.0	32.1	22	136.0	136.0
9	50.3	50.3	23	131.9	131.9
10	36.7	36.7	24	43.0	43.0
11	21.2	21.2	25	33.2	33.3
12	39.8	39.8	26	20.1	20.1
13	42.4	42.5	27	19.8	19.8
14	57.0	57.0	28	17.8	17.8

2.2. X-Ray Analysis. In order to confirm the absolute configuration of **1**, the crystal structure of its crystalline hydrate was investigated by X-ray diffraction analysis. Compound **1** crystallized in the Sohnke space group $P2_1$, with the asymmetric unit consisting of two dehydroergosterol molecules and two hydrate water molecules (Figure 2).

It follows from the data obtained that the bond lengths and bond angles in compound **1** are close to the usual ones [48]. Ring A takes a somewhat distorted chair conformation in the first (**1a**) and second (**1b**) crystallographically independent molecules (the minimum parameters of cycle asymmetry [49] and intracyclic torsion angles are given in Table 2). The conformation of cycle B in **1a** and **1b**, containing the C5=C6 double bond, is close to the slightly distorted 9α , 8-half-chair. The third carbocycle C in molecules **1a** and **1b** deviates more significantly from the ideal chair. The 5-membered cycle D in molecule **1a** takes the conformation of a 13β -envelope, strongly distorted towards the 14α , 13β -half-chair. In the second molecule **1b**, this cycle takes the conformation of the 14α , 13β -half-chair, strongly distorted towards the 13β -envelope. In general, distortions of the conformation of A-D cycles are close to those observed in the crystal structures of 3β -hydroxy- Δ^5 -sterols, for example, in 24 (R), 25-epoxycholesterol [50], stigmast-5-en-3-ol [51], (24E)-26-hydroxydesmosterol [52], and (24E)-26-hydroxydesmosterol monohydrate [53].

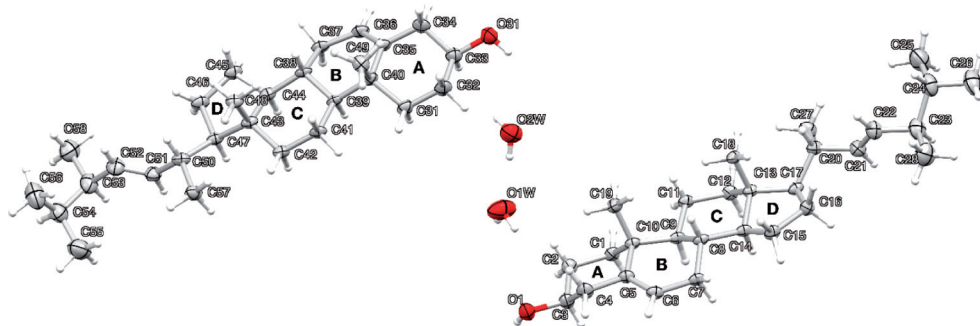


FIGURE 2: The asymmetric unit of the crystal structure of hydrate brassicasterol, with an atom labeling scheme. Thermal displacement ellipsoids are shown at the 50% probability level.

TABLE 2: Intracyclic torsion angles (τ , °) and asymmetry parameters (ΔC (min), °) in the structure of hydrate brassicasterol.

Crystallographically independent molecule 1a			Crystallographically independent molecule 1b		
Torsion angles	τ	ΔC	Torsion angles	T	ΔC
Cycle A					
C10-C1-C2-C3	-57.9 (4)	$\Delta C_S^2 = 2.3$	C40-C31-C32-C33	-59.1 (4)	$\Delta C_S^2 = 1.3$
C1-C2-C3-C4	57.0 (4)	$\Delta C_2^{2,3} = 2.7$	C31-C32-C33-C34	57.2 (4)	$\Delta C_2^{1,2} = 3.2$
C2-C3-C4-C5	-54.2 (4)		C32-C33-C34-C35	-52.2 (5)	
C3-C4-C5-C10	52.2 (4)		C33-C34-C35-C40	50.8 (4)	
C4-C5-C10-C1	-49.4 (4)		C34-C35-C40-C31	-50.1 (4)	
C2-C1-C10-C5	51.6 (4)		C32-C31-C40-C35	53.3 (4)	
Cycle B					
C10-C5-C6-C7	2.2 (5)	$\Delta C_2^{8,9} = 1.9$	C40-C35-C36-C37	2.0 (5)	$\Delta C_2^{8,9} = 2.0$
C5-C6-C7-C8	14.8 (5)		C35-C36-C37-C38	15.4 (5)	
C6-C7-C8-C9	-45.5 (3)		C36-C37-C38-C39	-46.5 (4)	
C7-C8-C9-C10	62.2 (3)		C37-C38-C39-C40	63.0 (3)	
C8-C9-C10-C5	44.1 (3)		C38-C39-C40-C35	-45.2 (4)	
C6-C5-C10-C9	12.5 (4)		C36-C35-C40-C39	12.8 (4)	
Cycle C					
C14-C8-C9-C11	-46.0 (3)	$\Delta C_S^9 = 4.3$	C44-C38-C39-C41	-48.5 (3)	$\Delta C_S^9 = 2.2$
C8-C9-C11-C12	45.3 (3)	$\Delta C_2^{9,11} = 4.7$	C38-C39-C41-C42	48.9 (4)	$\Delta C_2^{9,11} = 4.0$
C9-C11-C12-C13	-52.6 (4)		C39-C41-C42-C43	-54.4 (4)	
C11-C12-C13-C14	58.9 (3)		C41-C42-C43-C44	57.5 (3)	
C12-C13-C14-C8	-64.2 (3)		C42-C43-C44-C38	-60.4 (3)	
C9-C8-C14-C13	58.0 (3)		C39-C38-C44-C43	56.5 (3)	
Cycle D					
C17-C13-C14-C15	42.4 (3)	$\Delta C_S^{13} = 8.0$	C47-C43-C44-C45	46.0 (3)	$\Delta C_S^{13} = 14.0$
C13-C14-C15-C16	-30.3 (3)	$\Delta C_2^{13,14} = 11.8$	C43-C44-C45-C46	-35.5 (3)	$\Delta C_2^{13,14} = 4.9$
C14-C15-C16-C17	5.9 (3)		C44-C45-C46-C47	10.9 (4)	
C15-C16-C17-C13	19.9 (3)		C45-C46-C47-C43	17.4 (3)	
C14-C13-C17-C16	-37.4 (3)		C44-C43-C47-C46	-37.9 (3)	

In the crystal, molecules **1a** and **1b** and molecules of hydration water are linked by intermolecular hydrogen bonds (Table 3), forming infinite ribbons in the $(-1\ 0\ 2)$ plane along the b -axis (Figure 3).

2.3. Molecular Docking Studies. Four reasons motivated us to run molecular docking studies of ergosta-5, 22-dien-3 β -ol against the aromatase enzyme: first, the great structural similarity between ergosta-5, 22-dien-3 β -ol and the cocrystallized ligand (EXM) of the aromatase receptor (Figure 3); second, the reported cytotoxic effects of ergosterol derivatives; third, the reported anticancer effects of aromatase inhibitors [54]; and finally, the aromatase inhibition reports of some ergosterol

TABLE 3: Hydrogen-bond geometry for hydrate brassicasterol.

D-H...A	D-H...A	H...A (Å)	D...A (Å)	D...A (Å)
O1-H1... O2W ⁱ	0.84	1.87	2.703 (5)	175.3
O31-H31... O1 ⁱⁱ	0.84	2.09	2.869 (4)	155.1
O1W-H12W... O31 ⁱⁱⁱ	0.87	TJ2.11	2.875 (6)	146.3
O2W-H21W... O1 ^{iv}	0.87	1.95	2.812 (5)	171.2
O2W-H22W... O1W	0.87	1.96	2.821 (6)	172.8

Symmetry codes: (i) $x-1, y, z$; (ii) $x+1, y, z$; (iii) $-x+2, y+1/2, -z+1$; $-z+1$; (iv) $-x+1, y-1/2, -z+1$.

derivatives [38, 39]. In this work, molecular docking studies were carried out for ergosta-5, 22-dien-3 β -ol against aromatase (PDB ID: 3s7s) using the cocrystallized ligand as a reference

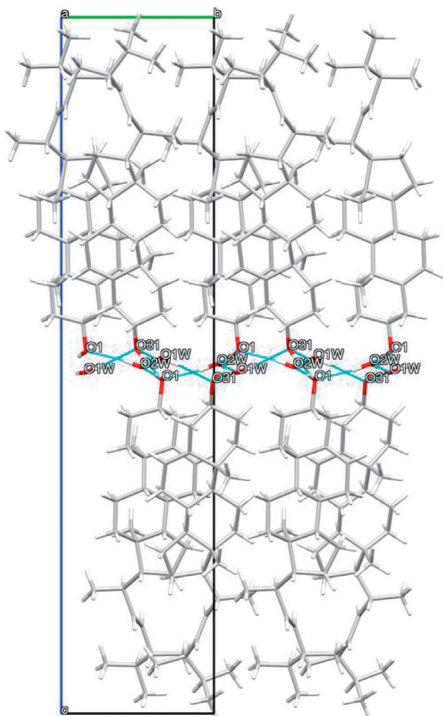


FIGURE 3: Packing diagram of the crystal structure of **1**, with indicated intramolecular hydrogen bonds between the dehydroergosterol OH-groups and hydrate water molecules.

molecule. We depended on the binding free energy (ΔG) and the correct binding mode between the docked molecules and the active site of aromatase. The binding free energies are summarized in Table 4.

At first, 3D-flexible alignment of ergosta-5, 22-dien-3 β -ol with the cocrystallized ligand (EXM) was carried out (Figure 4). From 3D-flexible alignment, it was observed that the structure of ergosta-5, 22-dien-3 β -ol has a good overlap with the cocrystallized ligand (EXM).

Then, validation of the docking process was checked through the running of the docking procedure for only the cocrystallized ligand (EXM) against the active pocket of aromatase. It was found that the produced RMSD value between the generated pose of the docked molecule and the original one equals 0.90. This indicates the validity of the docking process (Figure 5).

The binding mode of the cocrystallized ligand (EXM) as a reference molecule showed a binding free energy of -22.61 kcal/mol (Table 3). The binding interaction showed that the steroidal nucleus overlapped with the hydrophobic environment of the binding pocket of the aromatase receptor. The methyl group at position-13 formed two hydrophobic interactions with Leu477 and Val370. Besides, the C ring of steroidal moiety was involved in hydrophobic interactions with Ile133. The B ring was engaged in two hydrophobic interactions with Val370 and Cys437. The methyl group at position-10 formed two hydrophobic interactions with Cys437 and Val370. Finally, the methylene group at position-6 was involved in two hydrophobic interactions with Cys437 and Val373 (Figure 6).

TABLE 4: Binding free energies (ΔG in kcal/mol) of brassicasterol and cocrystallized ligand against aromatase.

Compound	ΔG [kcal/mol]
Cocrystallized ligand	-22.61
1	-33.55

Brassicasterol interacted with the active site of aromatase showing a binding mode almost the same as that of the cocrystallized ligand with extra hydrogen bonding and hydrophobic interactions. Ergosta-5, 22-dien-3 β -ol exerted a binding affinity of -33.55 kcal/mol, which was higher than that of the cocrystallized ligand. The binding mode revealed the orientation of the steroidal nucleus of the docked molecule toward the hydrophobic pocket of the aromatase receptor. The D ring of the steroidal moiety was involved in hydrophobic interaction with Val370, Val373, and Cys437. The methyl group at position-13 formed two hydrophobic interactions with Trp224 and Ile133. Also, the C ring of the steroidal moiety was involved in hydrophobic interaction with Ile133. The B ring was engaged in two hydrophobic interactions with Ile133 and Cys437. The A ring formed three hydrophobic interactions with Ile133, Ala306, and Cys437. The methyl group at position-10 formed two hydrophobic interactions with Cys437 and Ile133. The hydroxyl group at position-3 was involved in hydrogen bonding interaction with Gly349. Finally, the side chain (5, 6-dimethylhept-3-ene) moiety formed extra hydrophobic interactions with Val369, Val370, Leu477, Phe221, and Trp224 (Figure 7).

2.4. In Silico ADMET Analysis. ADMET studies were carried out for ergosta-5, 22-dien-3 β -ol and the cocrystallized ligand. Discovery studio 4.0 was used to predict ADMET descriptors for all compounds. The predicted descriptors are listed in Table 5.

The ADMET-Blood-Brain Barrier (BBB) penetration study predicted that ergosta-5, 22-dien-3 β -ol has a very low level of penetration indicating that ergosta-5, 22-dien-3 β -ol is safe against the central nervous system (CNS). ADMET aqueous solubility of ergosta-5, 22-dien-3 β -ol was very low, and andergosta-5, 22-dien-3 β -ol was predicted to have a poor level of intestinal absorption. CYP2D6 is involved in the metabolism process of a broad range of metabolites inside the liver [55]. Ergosta-5, 22-dien-3 β -ol was predicted as a noninhibitor of CYP2D6. Consequently, the liver dysfunction reaction is not expected upon administration of brassicasterol. The plasma protein binding model predicts whether a xenobiotic is highly bound ($>90\%$ bound) to carrier proteins in the blood [56]. Ergosta-5, 22-dien-3 β -ol was expected to bind plasma protein over than 90% (Figure 8).

2.5. In Silico Toxicity Studies. Toxicity prediction was carried out based on the validated and constructed models in Discovery studio software [57, 58] as follows: (i) FDA rodent carcinogenicity, (ii) rat maximum tolerated dose, (iii) rat oral median lethal dose (LD_{50}), (iv) rat chronic lowest

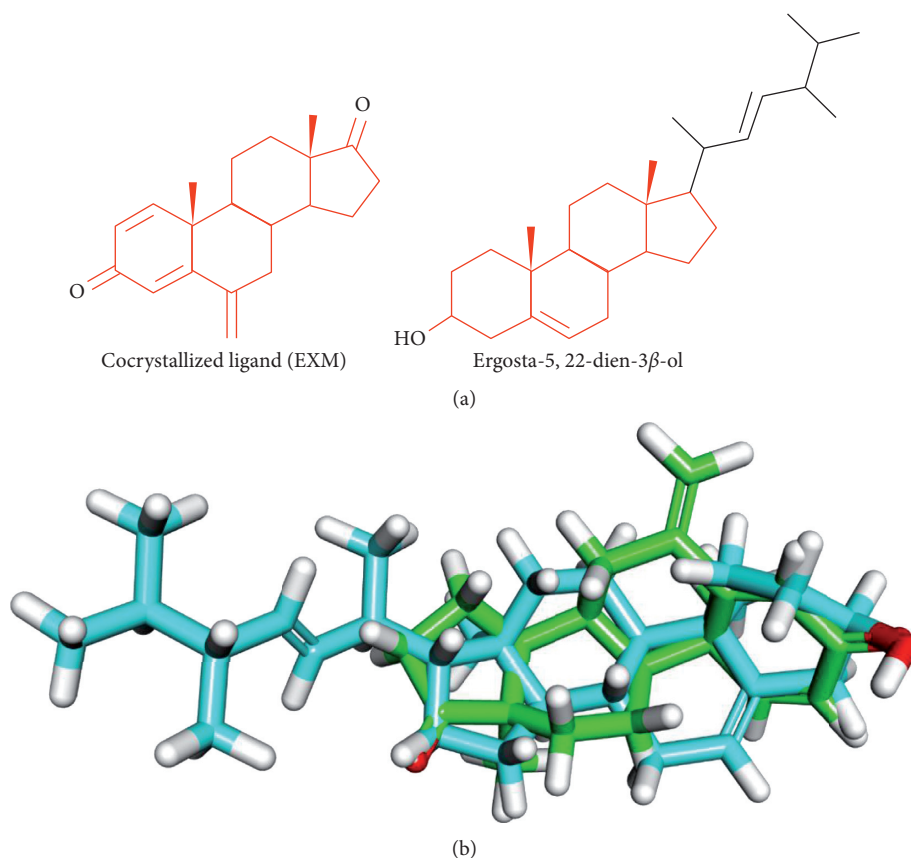


FIGURE 4: (a) Chemical structures and (b) flexible alignment of brassicasterol (carbon atoms in turquoise) with the cocrystallized ligand (EXM) (carbon atoms in green).

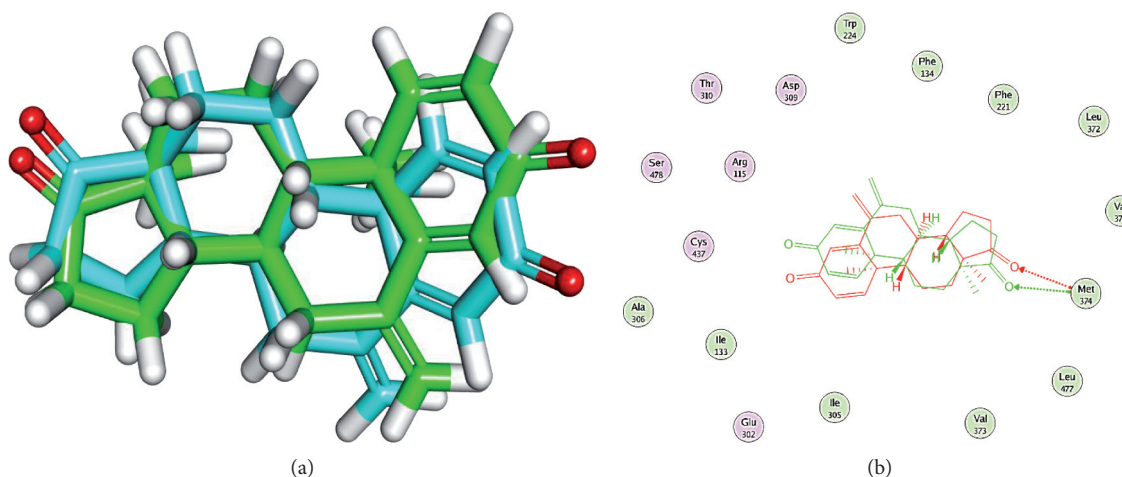


FIGURE 5: Superimposition of the cocrystallized molecule (green) and the docking pose (turquoise) of the same molecule.

observed adverse effect level (LOAEL), (v) ocular irritancy in the Draize test [59], and (vi) skin irritancy in a rabbit skin irritancy test [59]. As shown in Table 6, ergosta-5, 22-dien-3 β -ol showed *in silico* low adverse effects and toxicity against the tested models. Regarding FDA rodent carcinogenicity, ergosta-5, 22-dien-3 β -ol was predicted to be

noncarcinogenic. Regarding the rat maximum tolerated dose model, ergosta-5, 22-dien-3 β -ol showed a maximum tolerated dose value of 0.028 g/kg body weight which was higher than that of the cocrystallized ligand (0.026 g/kg body weight). Ergosta-5, 22-dien-3 β -ol showed a rat oral LD₅₀ value of 1.071 mg/kg body weight/day, which was less than of

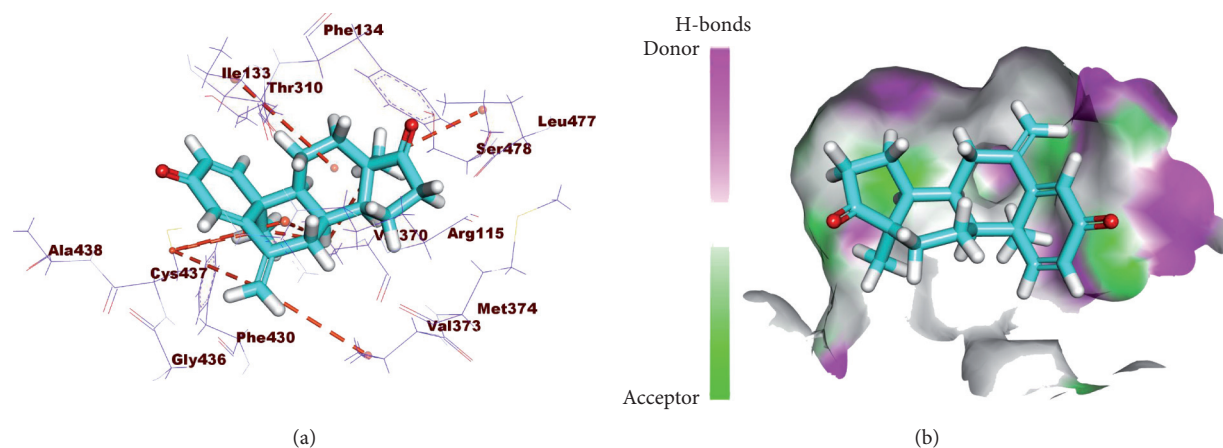


FIGURE 6: (a) 3D representation of the cocrystallized ligand (EXM) docked into the active site of aromatase. (b) Mapping surface showing the cocrystallized ligand (EXM) occupying the active pocket of aromatase.

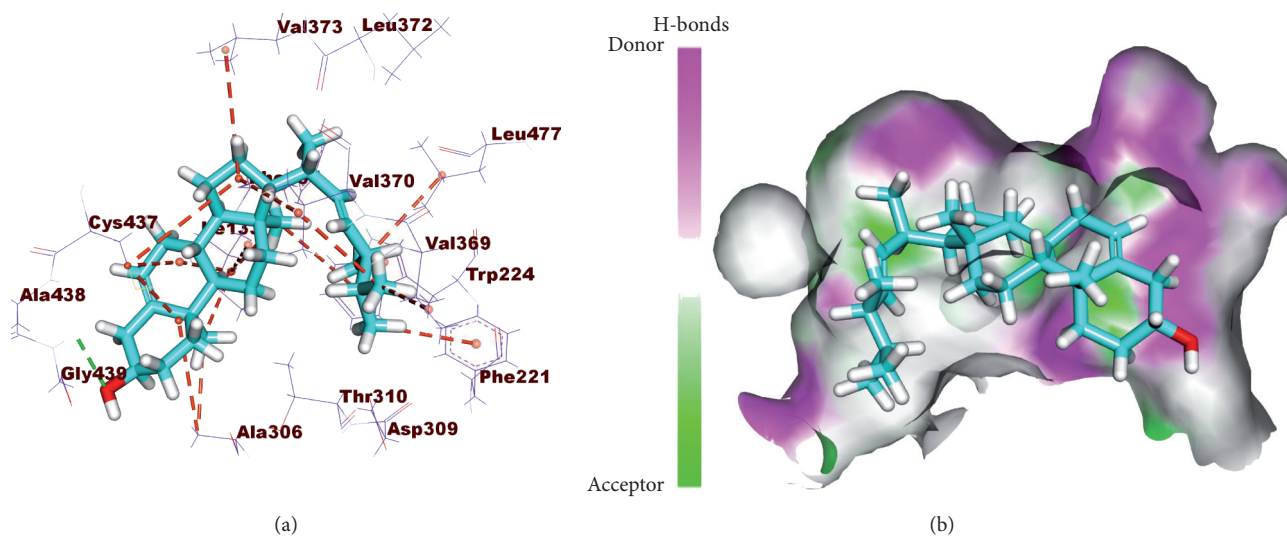


FIGURE 7: (a) 3D representation of brassicasterol docked into the active site aromatase. (b) Mapping surface showing ergosta-5, 22-dien-3 β -ol occupying the active pocket of aromatase.

TABLE 5: Predicted ADMET for the brassicasterol and reference drug.

Comp.	BBB level ^a	Solubility level ^b	Absorption level ^c	CYP2D6 prediction ^d	PPB prediction ^e
1	4	1	3	False	True
Cocrystallized ligand	1	2	0	False	True

^aBBB level, blood-brain barrier level, 0 = very high, 1 = high, 2 = medium, 3 = low, 4 = very low. ^bSolubility level, 1 = very low, 2 = low, 3 = good, 4 = optimal. ^cAbsorption level, 0 = good, 1 = moderate, 2 = poor, 3 = very poor. ^dCYP2D6, cytochrome P2D6, TRUE = inhibitor, FALSE = noninhibitor. ^ePPB, plasma protein binding, FALSE means less than 90%, TRUE means more than 90%.

the cocrystallized ligand (2.015 mg/kg body weight/day). For the rat chronic LOAEL model, ergosta-5, 22-dien-3 β -ol showed a LOAEL value less than the cocrystallized ligand.

Moreover, ergosta-5, 22-dien-3 β -ol was predicted to be irritant and moderately irritant against ocular irritancy and skin irritancy models, respectively.

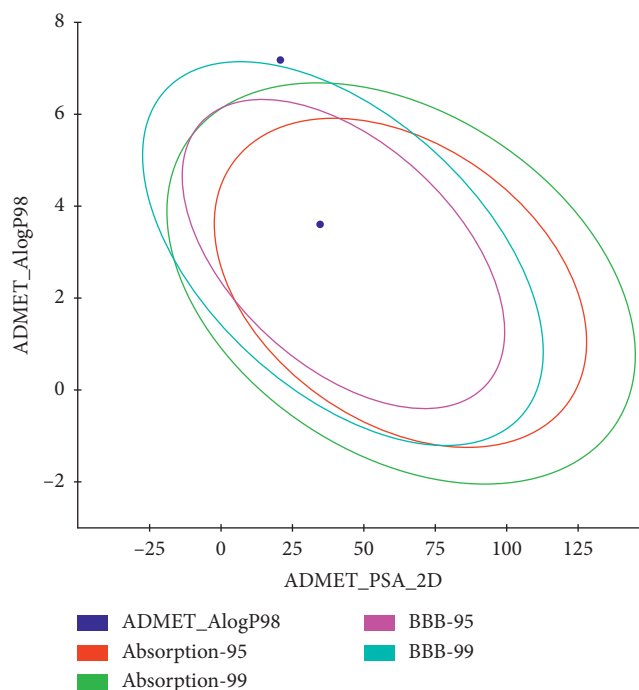


FIGURE 8: The expected ADMET study of brassicasterol.

TABLE 6: Toxicity properties of brassicasterol and the cocrystallized ligand.

Compound	FDA rodent carcinogenicity (rat-male)	Rat maximum tolerated dose (feed) ^b	Rat oral LD ₅₀ ^b	Rat chronic LOAEL ^b	Ocular irritancy	Skin irritancy
1	Noncarcinogen	0.028	1.071	0.002	Irritant	Moderate
Cocrystallized ligand	Noncarcinogen	0.026	2.015	0.015	Irritant	Moderate

^aUnit: mg/kg body weight/day. ^bUnit: g/kg body weight.

3. Experimental

3.1. Isolation of Brassicasterol (1). The raw material of *G. esculenta* was collected in summer in the vicinity of the city of Karkaraly, Karaganda Region, Kazakhstan. *G. esculenta* was extracted *via* adding 300 mL of MeOH to 207.5 g of a semidried powder and sonicated at 40–50°C for 3 hrs. The procedure was repeated 3 times per day. The obtained extracts were combined and evaporated under reduced pressure. Total weight of the obtained extract was 62.9 g.

The total extract was subjected to a SiO₂ column (400 g) using hexane–EtOAc and CH₂Cl₂–MeOH as mobile phases in a manner of increasing polarity. Pure white-colored crystal of **1** was obtained from fraction 54 (hexane–EtOAc 1 : 10).

3.2. X-Ray Analysis. X-ray intensity data for the compound C₂₈H₄₆O·H₂O were collected at 100 K, on a Rigaku Oxford Diffraction Supernova Dual Source (Cu at zero) diffractometer equipped with an Atlas CCD detector using ω scans and CuK α ($\lambda = 1.54184 \text{ \AA}$) radiation. The images were interpreted and integrated with the program CrysAlisPro [60]. Using Olex2 [61], the structure was solved by direct

methods using the ShelXT structure solution program and refined by full-matrix least squares on F [2] using the ShelXL program package [62, 63]. Nonhydrogen atoms were anisotropically refined, and the hydrogen atoms in the riding mode were with isotropic temperature factors fixed at 1.2 times U (eq) of the parent atoms (1.5 times for methyl and hydroxyl groups). The absolute configuration was established showing a refined Flack parameter of 0.0 (2).

CCDC-2060747 contains the supplementary crystallographic data for this paper. These data can be obtained free of charge from The Cambridge Crystallographic Data Centre via <http://www.ccdc.cam.ac.uk/structures>.

Details of the X-ray crystal structure data collection and refinement are given in Table 7.

3.3. In Silico Studies

3.3.1. Molecular Docking. The used software was Molecular Operating Environment (MOE) [64–67]. For more details, see the supplementary materials.

3.3.2. ADMET. ADMET descriptors of brassicasterol were computed by Discovery studio 4.0 20. More details are given in the supplementary materials.

TABLE 7: Crystal data and details of the data collection and structure refinement for hydrate brassicasterol.

Parameters	Hydrate brassicasterol
Empirical formula	C ₂₈ H ₄₆ O H ₂ O
Formula weight (g/mol)	416.66
Temperature (K)	100 (1)
Crystal system	Monoclinic
Space group	<i>P</i> 2 ₁
<i>a</i> (Å)	9.8621 (2)
<i>b</i> (Å)	7.5289 (2)
<i>c</i> (Å)	34.4423 (5)
β (°)	93.926 (1)
Volume (Å ³)	2551.37 (9)
<i>Z</i>	4
ρ_{calc} (g/cm ³)	1.085
μ (mm ⁻¹)	0.495
<i>F</i> (000)	928.0
Crystal size (mm ³)	0.351 × 0.129 × 0.072
Radiation	CuK α (λ = 1.54184)
2 Θ range for data collection (°)	7.718 to 150.484
<i>T</i> _{min} , <i>T</i> _{max}	0.760, 1.000
Index ranges	-12 ≤ <i>h</i> ≤ 12, -8 ≤ <i>k</i> ≤ 9, -40 ≤ <i>l</i> ≤ 43
Reflections collected	47210
Independent reflections	9920 [<i>R</i> _{int} = 0.0542, <i>R</i> _{sigma} = 0.0442]
Data/restraints/parameters	9920/1/561
Goodness-of-fit on <i>F</i> ²	1.037
Final <i>R</i> indexes [<i>I</i> ≥ 2 σ (<i>I</i>)]	<i>R</i> ₁ = 0.0738, <i>wR</i> ₂ = 0.1944
Final <i>R</i> indexes [all data]	<i>R</i> ₁ = 0.0773, <i>wR</i> ₂ = 0.1994
Largest diff. peak/hole (e ⁻ Å ⁻³)	0.54/-0.34
Flack parameter	0.0 (2)

3.3.3. *In Silico Toxicity.* Discovery studio 4.0 was used to calculate the toxicity parameters of brassicasterol [25]. For more details, see the supplementary materials.

4. Conclusions

Ergosta-5, 22-dien-3 β -ol (**1**) was isolated from a methanol extract of the fungus *Gyromitra esculenta*. The absolute configuration of **1** was determined by X-ray structural crystallography. Ergosta-5, 22-dien-3 β -ol occupied the binding site of the aromatase enzyme with a binding mode very similar to that of the cocrystallized ligand and a binding affinity of -33.55 kcal/mol, which was higher than that of the cocrystallized ligand (-22.61 kcal/mol). *In silico* ADMET and toxicity studies against 6 models have been conducted, and the results expected the safety of **1** with a disadvantage of poor water solubility and absorption.

Data Availability

Details of the *in silico* experimental part and NMR data of compound **1** are available in the supplementary data. Also, CCDC-2060747 contains the supplementary crystallographic data for this paper. These data can be obtained free of charge via <https://www.ccdc.cam.ac.uk/structures>.

Conflicts of Interest

The authors declare no conflicts of interest.

Authors' Contributions

Yerlan Melsuly Suleimen was responsible for collection of raw material, extraction of raw material, isolation of compounds, and identification of spectra. Ahmed M. Metwaly contributed to identification of spectra and doking studies of the compound. Ahmad E. Mostafa and Eslam B. Elkaeed contributed to doking studies of the compound. Hong-wei Liu and Buddha Bahadur Basnet took part in isolation of compound. Raigul Nurbekkyzy Suleimen was responsible for identification of spectra. Margarita Yulayevna Ishmuratova contributed to collection of raw material and identification of mushroom. Koblandy Muboryakovich Turdybekov took part in interpretation of X-ray analysis. Kristof Van Hecke was responsible for X-ray analysis and interpretation of results of it.

Acknowledgments

This research was funded by the Science Committee of the Ministry of Education and Science of the Republic of Kazakhstan (Grant no. AP08051842, and the grant name is «Creation and replenishment of the collection of industrially valuable microorganisms, study and preservation of their biological diversity for the needs of biotechnology, medicine, and agriculture») and by the Chinese Academy of Science (Grant PIFI). The authors thank Dr. M.Yu. Ishmuratova (Professor of E.A. Buketov Karagandy University, Republic of Kazakhstan) for assistance in determining the plant species. K.V.H. thanks the Research Foundation–Flanders (FWO) (projects AUGÉ/11/029 and G099319N) for funding.

Supplementary Materials

Figure S1: 1H-NMR (500 MHz, CDCl₃) spectrum of **1**. Figure S2: 13C-NMR (125 MHz, CDCl₃) spectrum of **1**. Figure S3: DEPT (125 MHz, CDCl₃) spectrum of **1**. Figure S4: 1H–1H Cosy (500 MHz, CDCl₃) spectrum of **1**. Figure S5: HMQC spectrum of **1**. Figure S6: HMBC spectrum of **1**. (*Supplementary Materials*)

References

- [1] X. Han, Y. Yang, A. M. Metwaly, Y. Xue, Y. Shi, and D. Dou, "The Chinese herbal formulae (Yitangkang) exerts an anti-diabetic effect through the regulation of substance metabolism and energy metabolism in type 2 diabetic rats," *Journal of Ethnopharmacology*, vol. 239, Article ID 111942, 2019.
- [2] A. M. Metwaly, M. M. Ghoneim, I. H. Eissa et al., "Traditional ancient Egyptian medicine: A review," *Saudi Journal of Biological Sciences*, 2021, in Press.
- [3] M. H. Sharaf, G. M. El-Sherbiny, S. A. Moghannem et al., "New combination approaches to combat methicillin-resistant *Staphylococcus aureus* (MRSA)," *Scientific Reports*, vol. 11, pp. 1–16, 2021.
- [4] V. O. Imieje, A. A. Zaki, A. M. Metwaly et al., "Anti-leishmanial derivatives of humulene from *Asteriscus*

- hierochunticus with in silico tubulin inhibition potential," *Records of Natural Products*, 2021.
- [5] S. V. Sperstad, T. Haug, H.-M. Blencke, O. B. Styrvold, C. Li, and K. Stensvåg, "Antimicrobial peptides from marine invertebrates: challenges and perspectives in marine antimicrobial peptide discovery," *Biotechnology Advances*, vol. 29, no. 5, pp. 519–530, 2011.
- [6] A. El-Demerdash, A. M. Metwaly, A. Hassan et al., "Comprehensive virtual screening of the antiviral potentialities of marine polycyclic guanidine alkaloids against SARS-CoV-2 (COVID-19)," *Biomolecules*, vol. 11, no. 3, p. 460, 2021.
- [7] A. M. Metwaly, A. S. Wanas, M. M. Radwan, S. A. Ross, and M. A. ElSohly, "New α -Pyrone derivatives from the endophytic fungus *Embellisia* sp.," *Medicinal Chemistry Research*, vol. 26, no. 8, pp. 1796–1800, 2017.
- [8] A. Metwaly, H. Kadry, A. El-Hela, A. Elsalam, and S. Ross, "New antimalarial benzopyran derivatives from the endophytic fungus *Alternaria phragmospora*," *Planta Medica*, vol. 80, p. PC11, 2014.
- [9] A. Metwaly, "Comparative biological evaluation of four endophytic fungi isolated from *nigella sativa* seeds," *Al-Azhar Journal of Pharmaceutical Sciences*, vol. 59, no. 1, pp. 123–136, 2019.
- [10] R. I. Jalmakhanbetova, Ye. M. Suleimen, I. H. Eissa et al., "Isolation and biological evaluation of roseofungin and its cyclodextrin inclusion complexes," *Bulletin of Karaganda University*, vol. 4, no. 100, pp. 35–44, 2020.
- [11] B. B. Basnet, L. Liu, B. Chen et al., "Four new cytotoxic arborinane-type triterpenes from the endolichenic fungus *myrothecium inundatum*," *Planta Medica*, vol. 85, pp. 701–707, 2019.
- [12] B. B. Basnet, B. Chen, Y. M. Suleimen et al., "Cytotoxic secondary metabolites from the endolichenic fungus *hypoxylon fuscum*," *Planta Medica*, vol. 85, no. 13, pp. 1088–1097, 2019.
- [13] B. Buddha Bahadur, B. Chen, Y. M. Suleimen et al., "Cytotoxic secondary metabolites from the endolichenic fungus *Hypoxylon fuscum*," *Planta Medica*, vol. 85, pp. 1088–1097, 2019.
- [14] M. M. Ghoneim, W. M. Afifi, M. Ibrahim et al., "Biological evaluation and molecular docking study of metabolites from *Salvadora Persica L.* growing in Egypt," *Pharmacognosy Magazine*, vol. 15, p. 232, 2019.
- [15] L. Liu, S. Luo, M. Yu et al., "Chemical constituents of *tagetes patula* and their neuroprotecting action," *Natural Product Communications*, vol. 15, Article ID 1934578X20974507, 2020.
- [16] Y.-M. Wang, X.-K. Ran, M. Riaz et al., "Chemical constituents of stems and leaves of *tagetespatula L.* and its fingerprint," *Molecules*, vol. 24, no. 21, p. 3911, 2019.
- [17] A. S. Zhanzhaxina, M. Seilgazy, R. I. Jalmakhanbetova et al., "Flavonoids from *pulicaria vulgaris* and their antimicrobial activity," *Chemistry of Natural Compounds*, vol. 56, no. 5, pp. 915–917, 2020.
- [18] A. M. Yassin, N. M. El-Deeb, A. M. Metwaly, G. F. El Fawal, M. M. Radwan, and E. E. Hafez, "Induction of apoptosis in human cancer cells through extrinsic and intrinsic pathways by balanites aegyptiaca furostanol saponins and saponin-coated silvernanoparticles," *Applied Biochemistry and Biotechnology*, vol. 182, no. 4, pp. 1675–1693, 2017.
- [19] A. M. Metwaly, Z. Lianlian, H. Luqi, and D. Deqiang, "Black ginseng and its saponins: preparation, phytochemistry and pharmacological effects," *Molecules*, vol. 24, no. 10, p. 1856, 2019.
- [20] M. S. Alesawy, A. E. Abdallah, M. S. Taghour, E. B. Elkaeed, I. H. Eissa, and A. M. Metwaly, "In silico studies of some isoflavonoids as potential candidates against COVID-19 targeting human ACE2 (hACE2) and viral main protease (mpro)," *Molecules*, vol. 26, no. 9, p. 2806, 2021.
- [21] R. I. Jalmakhanbetova, Y. M. Suleimen, M. Oyama et al., "Isolation and in silico anti-COVID-19 main protease (Mpro) activities of flavonoids and a sesquiterpene lactone from *Artemisia sublessingiana*," *Journal of Chemistry*, vol. 2021, Article ID 5547013, 8 pages, 2021.
- [22] R. I. Jalmakhanbetova, E. B. Elkaeed, I. H. Eissa, A. M. Metwaly, and Y. M. Suleimen, "Synthesis and molecular docking of some grossgemin amino derivatives as tubulin inhibitors targeting colchicine binding site," *Journal of Chemistry*, vol. 2021, Article ID 5586515, 10 pages, 2021.
- [23] A. M. Metwaly, F. R. Fronczek, G. Ma et al., "Antileukemic α -pyrone derivatives from the endophytic fungus *Alternaria phragmospora*," *Tetrahedron Letters*, vol. 55, no. 24, pp. 3478–3481, 2014.
- [24] A. M. Metwaly, M. M. Ghoneim, and A. Musa, "Chance fracture," *Diagnostic Imaging: Spine*, vol. 7, pp. 322–327, 2015.
- [25] A. El-Demerdash, A. M. Metwaly, A. Hassan et al., "Comprehensive virtual screening of the antiviral potentialities of marine polycyclic guanidine alkaloids against SARS-CoV-2 (COVID-19)," *Biomolecules*, vol. 11, no. 3, p. 460, 2021.
- [26] A. M. Metwaly, H. A. Kadry, A. A. El-Hela et al., "Nigrosphaerin A a new isochromene derivative from the endophytic fungus *Nigrospora sphaerica*," *Phytochemistry Letters*, vol. 7, pp. 1–5, 2014.
- [27] B. Nicholson and F. H. Brightman, *The Oxford Book of Flowerless Plants*, Oxford University Press, Oxford, UK, 1974.
- [28] D. Minter, *IMI Descriptions of Fungi and Bacteria*, CABI, Wallingford, UK, 2018.
- [29] M. Härkönen, "Uses of mushrooms by Finns and Karelians," *International Journal of Circumpolar Health*, vol. 57, pp. 40–55, 1998.
- [30] I. Karkocha and H. Mlodecki, "Subject index," *Solid State Physics*, vol. 13, pp. 473–482, 1962.
- [31] M. Wu, T. Huang, J. Wang et al., "Antitumor effect of ergosterol and cisplatin-loaded liposomes modified with cyclic arginine-glycine-aspartic acid and octa-arginine peptides," *Medicine*, vol. 97, 2018.
- [32] X. Li, Q. Wu, Y. Xie et al., "Ergosterol purified from medicinal mushroom *Amauroderma rude* inhibits cancer growth in vitro and in vivo by up-regulating multiple tumor suppressors," *Oncotarget*, vol. 6, no. 19, pp. 17832–17846, 2015.
- [33] J.-H. Kang, J.-E. Jang, S. K. Mishra et al., "Ergosterol peroxide from Chaga mushroom (*Inonotus obliquus*) exhibits anti-cancer activity by down-regulation of the β -catenin pathway in colorectal cancer," *Journal of Ethnopharmacology*, vol. 173, pp. 303–312, 2015.
- [34] W. Tan, M. Pan, H. Liu, H. Tian, Q. Ye, and H. Liu, "Ergosterol peroxide inhibits ovarian cancer cell growth through multiple pathways," *OncoTargets and Therapy*, vol. 10, pp. 3467–3474, 2017.
- [35] L. Zheng, Y. S. Wong, M. Shao, S. Huang, F. Wang, and J. Chen, "Apoptosis induced by 9, 11-dehydroergosterol peroxide from *Ganoderma lucidum* mycelium in human malignant melanoma cells is Mcl-1 dependent," *Molecular Medicine Reports*, vol. 18, pp. 938–944, 2018.
- [36] L. Zheng, J. Si, and Y.-S. Wong, "Ergosterol peroxide and 9, 11-dehydroergosterol peroxide from *Ling Zhi* or *Reishi* medicinal mushroom, *Ganoderma lucidum* (W. Curt.: Fr.) P. Karst. (Aphyllophoromycetidae) mycelia inhibit the growth

- of human breast adenocarcinoma MCF-7 cells," *International Journal of Medicinal Mushrooms*, vol. 11, no. 3, 2009.
- [37] Y.-J. Cui, S.-H. Guan, L.-X. Feng et al., "Cytotoxicity of 9,11-dehydroergosterol peroxide isolated from *Ganoderma lucidum* and its target-related proteins," *Natural Product Communications*, vol. 5, Article ID 1934578X1000500806, 2010.
- [38] T. Kikuchi, N. Motoyashiki, T. Yamada et al., "Ergostane-type sterols from king trumpet mushroom (*pleurotus eryngii*) and their inhibitory effects on aromatase," *International Journal of Molecular Sciences*, vol. 18, no. 11, p. 2479, 2017.
- [39] R. F. A. Abdelhameed, E. S. Habib, M. S. Goda et al., "Thalassosterol, a new cytotoxic aromatase inhibitor ergosterol derivative from the red sea seagrass *thalassodendron ciliatum*," *Marine Drugs*, vol. 18, no. 7, p. 354, 2020.
- [40] H. W. Hircher and F. U. Rosenstein, "Isolation of brassicasterol from steam deodorizer distillate of rapeseed oil: some properties of its acetate tetrabromide and its reduction to 22, 23-dihydrobrassicasterol," *Lipids*, vol. 8, no. 8, pp. 453–458, 1973.
- [41] T. Matsumoto, N. Shimizu, T. Shigemoto, T. Itoh, T. Iida, and A. Nishioka, "Isolation of 22-dehydrocampesterol from the seeds of *brassica juncea*," *Phytochemistry*, vol. 22, no. 3, pp. 789–790, 1983.
- [42] P. Gladu, G. Patterson, G. Wikfors, D. Chitwood, and W. Lusby, 1990.
- [43] L. J. Goad and N. Withers, "Identification of 27-nor-(24R)-24-methylcholesta-5,22-dien-3 β -ol and brassicasterol as the major sterols of the marine dinoflagellate *Gymnodinium simplex*," *Lipids*, vol. 17, no. 12, pp. 853–858, 1982.
- [44] M. D. García, M. T. Sáenz, M. A. Gómez, and M. A. Fernández, "Topical antiinflammatory activity of phytosterols isolated from *Eryngium foetidum* on chronic and acute inflammation models," *Phytotherapy Research*, vol. 13, no. 1, pp. 78–80, 1999.
- [45] Y. Yazawa, N. Ikarashi, M. Hoshino, H. Kikkawa, F. Sakuma, and K. Sugiyama, "Inhibitory effect of ergosterol on bladder carcinogenesis is due to androgen signaling inhibition by brassicasterol, a metabolite of ergosterol," *Journal of Natural Medicines*, vol. 74, no. 4, pp. 680–688, 2020.
- [46] M. S. Smyth and J. Martin, "X ray crystallography," *Molecular Pathology*, vol. 53, no. 1, pp. 8–14, 2000.
- [47] Y. Sun, Y. Lin, X. Cao, L. Xiang, and J. Qi, "Sterols from mytilidae show anti-aging and neuroprotective effects via anti-oxidative activity," *International Journal of Molecular Sciences*, vol. 15, no. 12, pp. 21660–21673, 2014.
- [48] F. H. Allen, O. Kennard, D. G. Watson, L. Brammer, A. G. Orpen, and R. Taylor, "Tables of bond lengths determined by X-ray and neutron diffraction. Part 1. Bond lengths in organic compounds," *Journal of the Chemical Society, Perkin Transactions 2*, vol. 2, no. 12, pp. S1–S19, 1987.
- [49] W. L. Duax and D. A. Norton, *Atlas of Steroid Structure*, Ifi/Plenum, New York, NY, USA, 1975.
- [50] N. C. O. Tomkinson, T. M. Willson, J. S. Russel, and T. A. Spencer, "Efficient, stereoselective synthesis of 24(S), 25-Epoxycholesterol," *The Journal of Organic Chemistry*, vol. 63, no. 26, pp. 9919–9923, 1998.
- [51] E. Moreno-Calvo, F. Temelli, A. Cordoba, N. Masciocchi, J. Veciana, and N. Ventosa, "A new microcrystalline phytosterol polymorph generated using CO₂-expanded solvents," *Crystal Growth & Design*, vol. 14, no. 1, pp. 58–68, 2014.
- [52] R. Saini, O. Kataeva, A. W. Schmidt et al., "Synthesis and biological activity of (24E)- and (24Z)-26-hydroxydesmosterol," *Bioorganic & Medicinal Chemistry*, vol. 21, no. 18, pp. 5794–5798, 2013.
- [53] G. R. Pettit, Y. Meng, D. L. Herald, K. A. N. Graham, R. K. Pettit, and D. L. Doubek, "Isolation and structure of ruprechstyril from *Ruprechtia tangarana*," *Journal of Natural Products*, vol. 66, no. 8, pp. 1065–1069, 2003.
- [54] P. E. Goss and K. Strasser, "Aromatase inhibitors in the treatment and prevention of breast cancer," *Journal of Clinical Oncology*, vol. 19, no. 3, pp. 881–894, 2001.
- [55] P. P. Roy and K. Roy, "QSAR studies of CYP2D6 inhibitor aryloxypropanolamines using 2D and 3D descriptors," *Chemical Biology & Drug Design*, vol. 73, no. 4, pp. 442–455, 2009.
- [56] T. Ghafourian and Z. Amin, "QSAR models for the prediction of plasma protein binding," *BioImpacts: BI*, vol. 3, p. 21, 2013.
- [57] X. Xia, E. G. Maliski, P. Gallant, and D. Rogers, "Classification of kinase inhibitors using a bayesian model," *Journal of Medicinal Chemistry*, vol. 47, no. 18, pp. 4463–4470, 2004.
- [58] BIOVIA QSAR, "ADMET and predictive toxicology," 2020, <https://www.3dsbiovia.com/products/collaborative-science/biovia-discovery-studio/qsar-admet-and-predictive-toxicology.html>.
- [59] K. R. Wilhelmus, "The draize eye test," *Survey of Ophthalmology*, vol. 45, no. 6, pp. 493–515, 2001.
- [60] O. D. Rigaku, *Crysalis Pro*, Rigaku Oxford Diffraction, Yarnton, UK, 2018.
- [61] O. V. Dolomanov, L. J. Bourhis, R. J. Gildea, J. A. K. Howard, and H. Puschmann, "OLEX2: a complete structure solution, refinement and analysis program," *Journal of Applied Crystallography*, vol. 42, no. 2, pp. 339–341, 2009.
- [62] G. M. Sheldrick, "Crystal structure refinement with SHELXL," *Acta Crystallographica Section C Structural Chemistry*, vol. 71, no. 1, pp. 3–8, 2015.
- [63] G. M. Sheldrick, "A short history of SHELX," *Acta Crystallographica Section A Foundations of Crystallography*, vol. 64, no. 1, pp. 112–122, 2008.
- [64] N. Martins, S. Petropoulos, and I. C. F. R. Ferreira, "Chemical composition and bioactive compounds of garlic (*Allium sativum* L.) as affected by pre- and post-harvest conditions: a review," *Food Chemistry*, vol. 211, pp. 41–50, 2016.
- [65] I. H. Eissa, A.-G. A. El-Helby, H. A. Mahdy et al., "Discovery of new quinazolin-4 (3H)-ones as VEGFR-2 inhibitors: design, synthesis, and anti-proliferative evaluation," *Bioorganic Chemistry*, vol. 105, Article ID 104380, 2020.
- [66] K. El-Adl, A.-G. A. El-Helby, R. R. Ayyad et al., "Design, synthesis, and anti-proliferative evaluation of new quinazolin-4 (3H)-ones as potential VEGFR-2 inhibitors," *Bioorganic & Medicinal Chemistry*, vol. 29, Article ID 115872, 2021.
- [67] A.-G. A. El-Helby, H. Sakr, R. R. Ayyad et al., "Design, synthesis, molecular modeling, in vivo studies and anticancer activity evaluation of new phthalazine derivatives as potential DNA intercalators and topoisomerase II inhibitors," *Bioorganic Chemistry*, vol. 103, Article ID 104233, 2020.